RESEARCH ARTICLE

Basalt Petrology, Water Chemistry, and Their Impact on the CO_2 Mineralization Simulation at Leizhou Peninsula Sites, Southern China

Jinglian Jiang[1,2], Pengchun Li[1,3], Changyou Xia[3], Jianxin Cai[1], Muxin Liu[3], Yongbin Jin[1] and Xi Liang[3,4]

Abstract

Mineral carbonation, which precipitates dissolved carbon dioxide (CO_2) as carbonate minerals in basaltic groundwater environments, is a potential technique for negative emissions. The Leizhou Peninsula in southwest Guangdong province has extensive basalt, indicating a promising potential for CO_2 storage through rapid mineralization. However, understanding of the basic geological setting, potential, and mechanisms of CO_2 mineralization in the basalts of the Leizhou Peninsula is still limited. The mineralization processes associated with CO_2 storage at two candidate sites in the area are investigated in this paper: Yongshi Farm and Tianyang Basin (of the dried maar lake). Petrography, rock geochemistry, basalt petrophysical properties, and groundwater hydrochemistry analyses are included in the study. Numerical simulation is used to examine the reaction process and its effects. The results show that basalts in the study areas mainly comprise plagioclase, pyroxene, and Fe–Ti oxides, revealing a total volume fraction exceeding 85%. Additionally, small amounts of quartz and fayalite are available, with volume fractions of 5.1% and 1.0%, respectively. The basalts are rich in divalent metal cations, which can form carbonate minerals, with an average of approximately 6.2 moles of metal cations per 1 kg of rock. The groundwater samples have a pH of 7.5–8.2 and are dominated by the Mg–Ca–HCO_3 type. The basalts demonstrate a porosity range of 10.9% to 28.8%, with over 70% of interconnected pores. A 20-year geochemical simulation revealed that CO_2 injection dissolves primary minerals, including anorthite, albite, and diopside, while CO_2 mineralization dissolves precipitation secondary minerals, such as calcite, siderite, and dolomite. Furthermore, a substantial rise in pH from 7.6 to 10.6 is observed in the vicinity of the injected well, accompanied by a slight reduction in porosity from 20% to 19.8%. Additionally, 36.8% of the injected CO_2 underwent complete mineralization within five years, revealing an increasing percentage of 66.1% if the experimental period is extended to 20 years. The presence of abundant divalent metal cations in basalts and water-bearing permeable rocks in the Leizhou Peninsula supports the potential for mineral carbonation in basalts, as indicated by the geochemical simulation results. Additional research is necessary to identify the factors that influence the CO_2 mineralization, storage, and sensitivity analysis of basalt in the Leizhou Peninsula.

Keywords CO_2 mineralization; Mineral carbonation; Basalt carbonation; Geochemistry simulation; Leizhou Peninsula

1 Introduction

Considerable amounts of greenhouse gases are released into the atmosphere through the burning of fossil fuels, such as coal, oil, and natural gas, and extensive deforestation, contributing to global warming. Carbon dioxide (CO_2) is the most important greenhouse gas (Bryant, 1997; Bachu and Adams, 2003). The appropriate disposal of CO_2 has become one of the most pressing challenges encountered today (Pacala et al., 2018). CO_2 geological storage is regarded as an effective method of large-scale CO_2 disposal in geological formations such as deep saline aquifers, oil and gas reservoirs, and unproductive coal seams (Bachu, 2015; Jia et al., 2019; Zhang and Ranjith, 2019). A low permeability or impermeable layer must be used as the upper cover for CO_2 geological storage to minimize the risk of CO_2 leakage after injection (Benson and Cole, 2008). Rutqvist et al. (2007) indicated that fluid-rock interactions and pressure changes induced by CO_2 injection may lead to the bursting of the capping layer. However, a safe and stable CO_2 storage technology that does not require a low-permeability cap layer may be suitable in areas with developed basalts

---

Article Highlights

- The geological and hydrological conditions of Leizhou Peninsula are verified to be suitable for CO_2 storage.
- Numerical model based on the actual geological condition is set to simulate CO_2 injection and storage in basalt layer.
- The concentration changes and migration processes of primary and secondary minerals are studied during the simulation.

✉ Pengchun Li
  lypengchun@scsio.ac.cn

1 Key Laboratory of Ocean and Marginal Sea Geology, South China Sea Institute of Oceanology, Chinese Academy of Sciences, Guangzhou 510301, China

2 University of Chinese Academy of Sciences, Beijing 100049, China

3 UK-China (Guangdong) CCUS Centre, Guangzhou 510440, China

4 University College London, London WC1E 6BT, United Kingdom

but lack effective caprock. This technology, which is known as CO_2 storage in basalts by mineralization technology (CSBM), includes CO_2 injection into rock layers. CO_2 reacts with minerals to produce carbonate minerals, facilitating the permanent storage of CO_2 (Pham et al., 2011; White et al., 2020).

The fundamental principle of CSBM lies in metal cations, such as Ca^{2+}, Mg^{2+}, and Fe^{2+}, which can combine with injected CO_2 upon their release from the rock under acidic conditions, thereby forming stable carbonate minerals. CO_2 is permanently fixed within the rock through the aforementioned process (Galeczka et al., 2014; Matter et al., 2009). The resulting carbonate minerals include ankerite, calcite, magnesite, and siderite. Several factors, such as the abundance of primary minerals in the rock, the dissolution rate and thermodynamic stability of the carbonate minerals, and the total solution fraction created by the carbonate minerals, influence the reaction (Aradóttir et al., 2011; Gislason et al., 2014). The dissolution of metal cations limits the course of the CO_2 mineralization reaction (Oelkers and Cole, 2008). Based on the reactivity and abundance of metal cations, mafic rocks (e.g., basalts) and ultramafic rocks (e.g., peridotites) are considered to be the most promising silicate minerals for CO_2 storage by mineralization (McGrail et al., 2006; Oelkers et al., 2008; Goldberg et al., 2008; Gislason et al., 2010). Basalts are a globally distributed rock type, occupying approximately 10% of the Earth's landmass and most of the ocean floor. Therefore, CSBM is regarded as one of the most promising technologies for large-scale carbon storage and application. Recent years have seen notable progress in theoretical analysis and implementation demonstration projects (Lu et al., 2011; Sanna et al., 2014; Snæbjörnsdóttir et al., 2014; Woodall et al., 2019). The CSBM demonstration projects in basalts worldwide currently include the CarbFix project in Iceland and the Wallula project in Washington, D.C. In particular, the CarbFix project has demonstrated the immediate capture of CO_2 injected with water through dissolution within 5 min. This project was the first to use tracer elements to monitor the process, revealing the complete mineralization of over 95% of the CO_2 injected into basalt formation and its sequestration in less than two years (Gislason et al., 2014; Snæbjörnsdóttir et al., 2020). The CarbFix demonstration project has been successfully implemented; thus, CBSM is the only mineral storage technology that has been field-tested and demonstrated to date (Li et al., 2022).

The Leizhou Peninsula has an extensive distribution of Quaternary basalts, covering over 3 000 km², which are either exposed to air or shallowly buried under unconsolidated Quaternary deposits. These basalts are an ideal test site for CO_2 storage through CSBM due to the lack of effective capping layers. The presence of several nearby CO_2 emission sources in the western part of Guangdong province, such as chemical plants and fossil-fuel-burning facto-

ries, enhances the experimental feasibility (Li et al., 2013; Chen et al., 2014; Li et al., 2023). The regional geological conditions, including the hydrochemical characteristics of groundwater (Kong, 2004; Lu et al., 2015; Wu et al., 2022; Zhang et al., 2020), as well as the petrology and geochemistry of basalts (Yu and O'Reilly, 2001; Han et al., 2009; Li et al., 2023), have been previously studied to identify suitable sites for CSBM pilot testing and demonstration in the Leizhou Peninsula. The CO_2 storage potential has also been assessed (Li et al., 2023). However, detailed work on the geological and hydrochemical interaction induced by CSBM in the Leizhou Peninsula, such as the dissolution of primary minerals and the precipitation of secondary minerals in the rock layers, which are essential elements in the geological simulation of in situ CO_2 mineralization, is still lacking (Hansen et al., 2005). A case study of a geological carbon storage site located on the Leizhou Peninsula, which is hosted by basaltic rock, is presented in this paper. This case study examines the potential reactions that may occur in response to CO_2 injection based on the conditions of basalts and groundwater hydrochemistry at the basaltic site in Leizhou Peninsula.

2 Geological setting

2.1 Regional geology

The Leizhou Peninsula is situated in the southwest of Guangdong province, China. This peninsula is bordered by the South China Sea to the east, the Qiongzhou Strait to the south, and the Beibu Gulf to the west. Geotectonically, the region is located in the utmost southwestern part of the Cathysian Plate, positioned at the forefront of the confluence of the Eurasian, Pacific, and Indo-Australian Plates (Tu et al., 1991). The peninsula has over 70 volcanic craters and cones, mostly in its southern part (Huang et al., 1993; Li et al., 2023). Based on the K-Ar dating method, the age range of these basalts is from 28.4 Ma to <0.1 Ma, with the majority formed during the Quaternary period (Huang and Cai, 1994; Ho et al., 2000). Quaternary volcanic eruptions generally comprise exposed volcanic rocks, covering a total distribution area of 3 136 km² (Huang et al., 1993). Fissure eruptions dominated volcanic activities during the Yanshanian period, while central eruptions were dominant during the Himalayan period. The volcanic rocks mainly comprise tholeiite, with less alkali basalt.

Three centers of Quaternary volcanic activity have been identified on the Leizhou Peninsula: Luogangling in the north, Jiashanling of Donghai and Naozhou Island in the east, and Shimaoling in the south (Huang et al., 1993). Basalt volcanoes in the north and south of the peninsula typically range from 20 m to 180 m in elevation. Shimaoling, standing at 259.3 m, is the highest point in the south-

ern region, while Luogangling is the highest point in the northern region at 233 m above sea level. The terraces are arranged around the volcanic cones and gradually decrease in elevation in a ladder-like pattern. These terraces have a flat topography with slopes of less than 5° and are situated in a transitional zone between steep canyons and gentle slopes.

2.2 Geology of candidate sites

Based on the characteristics of CO_2 storage in the basalts of the Leizhou Peninsula, particularly the general lack of depth and capping layer in Quaternary basalts, the dissolved CO_2 storage technology, known as CarbFix technology, was selected for the pilot test. Comprehensive analysis and investigation of five sites in the Leizhou Peninsula, namely, Luogangling, Huguangyan, Donghai Island in the north, and Tianyang Basin and Yongshi Farm in the south, revealed that the majority of the Quaternary basalts in the Leizhou Peninsula are not deeper than 200 m, which does not meet the minimum depth requirement to utilize the CarbFix technology. However, as the selected candidate sites, the Tertiary basalts in the Yongshi Farm and the caldera in Tianyang Basin demonstrated remarkable development. The geological conditions of the two selected sites are briefly described in the following section.

2.2.1 Tianyang basin site

The Tianyang Basin site is a maar lake basin situated at an average elevation of approximately 95.7 m. This basin, which is located near Tianyang Village, Xuwen County, was built on a relict caldera. The basin is a nearly elliptical depression with a length and width of approximately 4.1 and 3.1 km, respectively, extending from northwest to southeast (Yang et al., 2012). The shoulders of the basin have a height of approximately 20–50 m and steeper slopes (10°–20°) in the east, west, and south. The main volcanic rock units comprise pyroclastic rocks, especially tuff and breccia, from the Shimaoling Formation and lavas from the Xuwen Formation. The Tianyang Basin has an approximate age of 0.48 Ma and was formed during two periods of Early–Middle Pleistocene volcanism (Sui and Wang, 2003; Yang et al., 2006). Figure 1(a) displays spheroidal weathering on basalt field outcrops. The remaining basalt residue is porous due to gas eruption pores and fractures. Drill well 275 penetrates a basin filled with diatomaceous earth and peat soil up to 222 m thick. The basement comprises Shimaoling Formation volcanic rocks, with a thickness of over 265.12 m, as well as basaltic tuffs and lavas with abundant lapillus. Volcanic rocks contain abundant pores and fractures, and the matrix displays a vitreous to cryptocrystalline texture. Phenocrysts, including olivine and plagioclase, are also present. These characteristics are beneficial for mineralization storage, making volcanic rocks an ideal storage layer.

(a) Lapillus and blocks of basalts at the tianyang basin site
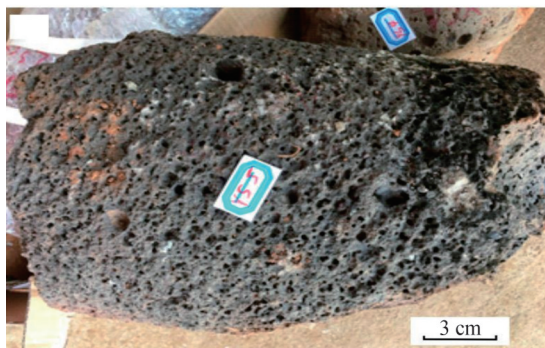
(b) Porous basaltic core samples from the yongshi farm site

(c) Drill cores of basalts at the yongshi farm site

Figure 1 Field outcrops and drill cores of basalts

2.2.2 Yongshi farm site

The Yongshi Farm, located in the northwestern part of Xuwen County, features volcanic cones and lava terraces. The region has a generally low relief, with elevations ranging from 160.0 m to 200.0 m, sloping slightly toward the north. Drill well 286 reveals a maximum thickness of 235.27 m of volcanic rocks in the area. The drill core of well 722 exhibits a 182.98 m sequence of volcanic rocks above a clastic sedimentary formation that is 208.96 – 450.83 m thick. At least six interlayers of basalt lavas are contained in the volcanic rock sequence, each ranging from 0.76 m to 26.69 m thick, totaling 52.91 m. The upper part of two drill holes penetrates the basalts of the Shimaoling period. The lithologies include basalt, hyalobasalt, and olivine basalt with blocky, porous, or fracture structures (Figures 1(b) and (c)) and partial serpentinization. The pores are unevenly distributed at different depths, but the basalt formations are often porous. Porous basalt comprises approximately 38% to 59% of the formations, increasing its potential as an effective storage layer.

3 Samples and methods

3.1 Mineralogical and chemical analysis methods

This study analyzed the mineralogical and chemical compositions of basalt core samples from Yongshi Farm and Tianyang Basin, as well as pyroclastic rock from Yingfengling, along with groundwater samples from Yongshi Farm as well as Yingfengling and Tianyang Basins. Five rock samples and four water samples were collected from Tianyang Basin; five rock samples and two water samples were collected from Yongshi Farm; and two rock samples and three water samples were collected from Yingfengling. Table 1 shows the specific information regarding the collection of rock and water samples on the Leizhou Peninsula. The goal was to model the mineralization process of CO_2 in porous basalt layers.

X-ray diffraction (XRD) analysis was conducted at the Key Laboratory of Ocean and Marginal Sea Geology, South China Sea Institute of Oceanology (SCSIO), Chinese Academy of Sciences (CAS), to detect the mineralogical composition of basalt samples. The samples were first pulverized to a 200 mesh size, and 50 g of aliquot was prepared for XRD analysis using a Bruker D8 ADVANCE X-ray diffractometer with Cu (monochrome) radiation. The equipment operated at a voltage of 40 kV and a current of 30 mA. Scanning was performed at an angle range of $2\theta = 3°–85°$ using a 1 mm slit and a scanning speed of 4°/min. Data deposition and processing were conducted using Jade 6.0 software. The chemical analysis of basalts was conducted at Nanjing FocuMS Technology Co. Ltd., China. Major elements were measured using the Agilent 5110 ICP–OES

Table 1 Specific information on rock and water samples

Sample sites	Sample name	Rock types	Latitude	Longitude
Yongshi farm	YS-1	Basalt core	20°29′14.415″	110°13′35.584″
	YS-1-2			
	YS-2			
	YS-3			
	YS-7			
Tianyang basin	TY-1	Basalt core	20°31′45.240″	110°17′11.987″
	TY-2			
	TY-3			
	TY-4			
	TY-10			
Yingfengling	YF01	Pyroclastic rock	20°34′52.465″	110°10′39.206″
	YF02			
Yongshi farm	YS01	Groundwater	20°31′59.796″	110°14′56.756″
	YS02	Groundwater	20°30′65.707″	110°13′86.691″
Tianyang basin	LSC-1	Groundwater	20°31′28″	110°17′20″
	LSC-2			
	LSC-3			
	LSC-4			
Yingfengling	YFL-1	Groundwater	20°34′55.163″	110°10′42.846″
	YFL-2			
	YFL-3			

instrument, while trace elements including rare earth elements (REEs), were measured using the Agilent 7700X ICP-MS instrument.

Among the nine underground water samples, three from the Yongshi Farm were nature spring water (YFL1-3), two were from the man-made well water of the Yongshi Farm with aquifer depths of 150 – 300 m (YS01-02), and four were well water with a depth of 70 m (LSC1-4) from the Tianyang Basin. The pH value was determined using the electrode method, and the concentration of iron ions was measured via o-phenanthroline spectrophotometry. Alkali cations, such as calcium, potassium, sodium, and magnesium, were measured using the inductively coupled plasma emission spectroscopy method. Mercury, arsenic, and selenium were measured using the atomic fluorescence method. The chemical analysis of the water was also conducted at the Key Laboratory of Ocean and Marginal Sea Geology, SCSIO, CAS.

3.2 Modeling

In terms of complex basalt volcano systems, the processes of CO_2 injection, storage by mineralization, and induced changes in geology, hydrology, and hydrochemistry remain unclear. Numerical simulation was used in this study to

analyze the mineral carbonate processes and mineralization efficiency to aid in our understanding. Specifically, CMG-GEM numerical simulation was adopted for the 400–450 m deep basaltic layer in the Yongshi Farm site, which was assumed to be homogeneous and serves as the target for CO_2 injection. A two-dimensional model section was created with a grid of 50×10, where horizontal and vertical grids represented 20 and 5 m, respectively, as shown in Figure 2. The left boundaries of the model contained a CO_2 injector and H_2O injector and the right contained an H_2O producer, respectively, thereby regulating the internal pressure of the model. The top and bottom of the model were defined as no-flux boundaries. The model calculations utilized the standard CMG database and measured sample data from the Leizhou Peninsula.

4 Results and discussions

4.1 Mineral composition and geochemistry

Basaltic outcrops are generally brown-black and are typically aphanitic, intersertal, and intergranular, showing felty textures. YS-1 from the Yongshi Farm site indicates an olivine phenocryst in a matrix of feldspar mud with a felty or interstitial texture (Figure 3(a)). YS-3 from the Yongshi Farm site shows partly altered olivine and fresh feldspar in an ophitic texture (Figure 3(b)). TY-2 from Tianyang Basin site shows an olivine phenocryst in a matrix of crystallite feldspar and olivine with typical intergranular texture (Figure 3(c)), and TY-10 from the Tianyang Basin site show partly and completely altered olivines in a felty matrix (Figure 3(d)). YF01 and YF02 weakly consolidated clastic rocks overlying basalts show sedimentary clots, basaltic clasts, and quartz (Figure 3(e) and (f)). In this context, the primary minerals include plagioclase, olivine, pyroxene, and Fe–Ti oxides, as shown in Figure 3. Some of

these minerals may undergo high-temperature re-equilibrium reactions, resulting in the partial or complete replacement of olivine by iddingsite (Figures 3(b) and (d), respectively). The XRD results further indicate that feldspar, olivine, and pyroxene are dominated by plagioclase series, fayalite, and diopside and hedenbergite, respectively. Additionally, XRD detected small amounts of high-temperature cristobalite (Table 2), indicating a frozen disequilibrium state in the rocks, which was not visible in the microscopic photos.

The basalts in Yongshi Farm mainly comprise bytownite, andesine, labradorite, anorthite, and albite as the main minerals, accompanied by a small amount of hedenbergite, and the average volume fractions of these minerals are 23.0%, 20.5%, 19.6%, 18.4%, 14.4%, and 4.2%, respectively. The basalts in the Yingfengling comprise graphite, andesine, labradorite, and quartz as the main minerals, with average mineral volume fractions of 30.5%, 27.1%, 23.5%, and 13.5%, respectively, accompanied by a small amount of cubanite and ludjibaite. The basalts in the Tianyang Basin area mainly comprise labradorite, andesine, oligoclase, diopside, cristobalite and fayalite, with average volume fractions of minerals being 33.7%, 33.1%, 23.9%, 6.6%, 1.3%, and 1.3%, respectively.

The entire composition results of major rock elements are listed in Table 3, and the trace elements are presented in Table 4. The contents of SiO_2 ranged from 46% to 54%. The total alkali content ($Na_2O + K_2O$) ranged from 1.76% to 4.57%. Based on the TAS plot, which refers to Bas et al. (1986), these rocks span from basalt to basaltic andesite in composition (Figure 4(a)). The Yongshi Farm is dominated by basalt and, to a lesser extent, basaltic andesite; the Tianyang Basin is dominated by basalt; and Yingfengling is predominantly in an area of basaltic andesite. All samples from Yingfengling are in the andesite region; most of the Yongshi Farm samples are within the alkaline basalt region; a few of the Tianyang Basin samples are in the alkaline basalt region; and the remaining samples are in the andesite region due to severe weathering (Figure 4(b)). The
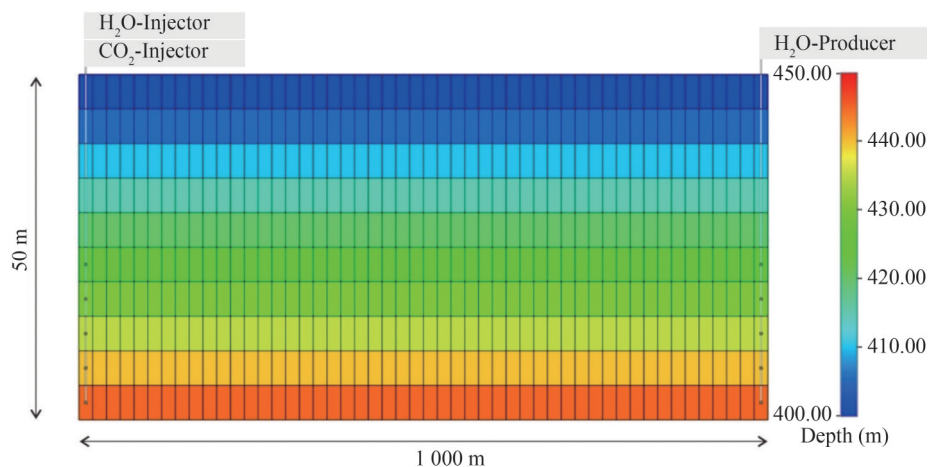
Figure 2 2D model for CO_2 mineralization process simulation in basalts based on the Yongshi Farm site

(a) YS-1

(b) YS-3

(c) TY-2

(d) TY-10

(e) YF01

(f) YF02
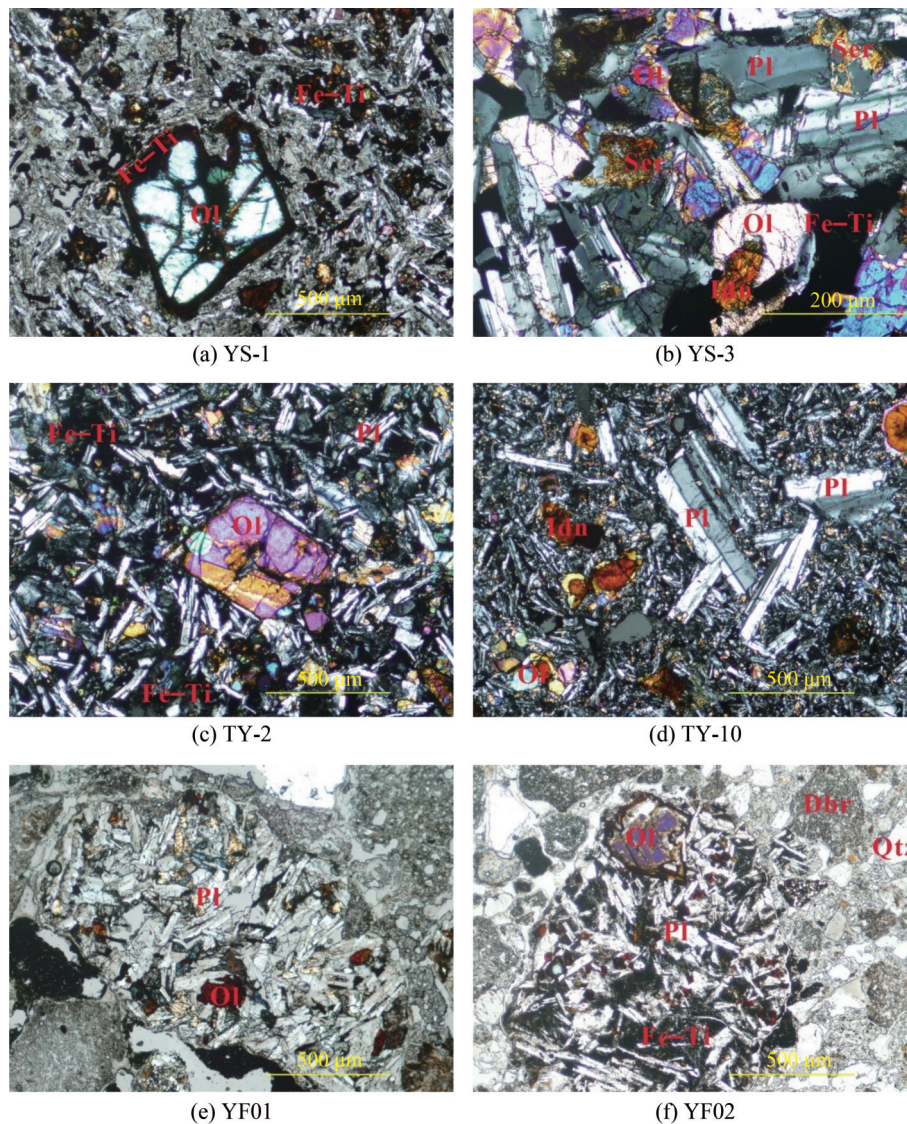
Figure 3 Photomicrographs under cross-polarization showing the mineral composition and structure of basalts. Abbreviations: Idn, iddingsite; Ol, olivine; Pl, plagioclase; Qtz, quartz; Ser, sericite; Dbr, debris; Fe–Ti, Fe and Ti-bearing oxides

Cenozoic basalts are mostly quartz and olivine basalt, revealing a few alkaline basalts. The main divalent cationic oxides of the minerals are CaO, MgO, and Fe_2O_3, accounting for 16%–24% of the rock. The concentration of MnO is 0.14%–0.24%. The basalts of the Leizhou Peninsula have low K_2O (0.2%–1.08%), low P_2O_5 (0.137%–0.308%), and high SiO_2 (46.869%–54.037%). The loss on ignition (LOI) ranges from 4.6% to 14.1%, indicating possible water content variations due to the general absence of deuteric alteration. Overall, the alkali olivine basalts are characterized by high levels of K_2O and P_2O_5 and low levels of SiO_2. By contrast, quartz tholeiites have relatively low levels of K_2O and P_2O_5 but high levels of SiO_2. Olivine tholeiites have K_2O and P_2O_5 levels that fall between the two. Basaltic pyroclastic rocks demonstrate the highest SiO_2 levels. The MgO content of the samples varies widely, ranging from

2.449% to 6.572% in basaltic pyroclastic rocks and alkaline olivine basalts, respectively.

The trace element contents in rocks from three different regions demonstrate similar trends, with high-field strength elements such as Nb, Ta, and Ti (Figure 5(a)) and the normalizing values of chondrite from McDonough and Sun (1995). The REE distribution, normalized to chondrite (Figure 5(b)), displays a predominantly right-inclined pattern with no or weak positive europium (Eu) anomalies, similar to ocean island basalts. This similarity indicates magma eruption from the mantle to the surface along the tectonic rift without stable crystalline differentiation, which is a crucial feature of rift volcanism. This result further confirms the history of rift volcanism on the Leizhou Peninsula. The overall fractionated medium and heavy rare earth elements indicate a magma source within the garnet stability

Table 2 Primary minerals in basalt samples analyzed by XRD and the secondary minerals set in the model

Sample	Primary minerals													
	Ab	Ads	An	Byt	Crs	Cub	Di	Fa	Grp	Hd	Lab	Lud	Olg	Qtz
YS-1	11.3	27.0	17.4	18.7						4.2	21.4			
YS-1-2	16.0	16.7	20.3	22.0						8.0	17.1			
YS-2	17.2	18.6	18.5	23.7						3.2	18.8			
YS-3	10.4	22.2	15.2	27.2						2.5	22.6			
YS-7	16.9	17.9	20.7	23.2						3.0	18.2			
Aver	14.4	20.5	18.4	23.0						4.2	19.6			
YF01		26.8				2.4			34.5		17.7	2.6		16.0
YF02		27.3				3.1			26.4		29.3	2.9		10.9
Aver		27.1				2.8			30.5		23.5	2.8		13.5
TY-2		32.3			1.6		6.6	1.2			33.0		25.3	
TY-3		33.1			1.6		5.0	1.3			32.8		26.2	
TY-4		30.8			1.1		7.2	1.3			31.6		28.0	
TY-5		33.7			1.4		7.1	1.4			35.5		20.9	
TY-10		35.7			1.0		7.3	1.4			35.5		19.2	
Aver		33.1			1.3		6.6	1.3			33.7		23.9	
Secondary minerals														
	Cal	Daw	Dol	Mgs	Sd									
	0.0	0.0	0.0	0.0	0.0									

Note: The blanks represent that the mineral is undetected or has a very small volume fraction.

Table 3 Results of major element composition (wt.%) of overall rock of basalts samples from the candidate sites in the Leizhou Peninsula

Sample	Sample site	Rock type	SiO_2	Al_2O_3	MgO	Na_2O	K_2O	P_2O_5	TiO_2	CaO	Fe_2O_3	MnO	LOI	Total
YS-1	Yongshi farm	QT	51.950	16.555	3.187	2.798	1.086	0.306	1.565	4.522	12.767	0.176	5.460	100.373
YS-1-2	Yongshi farm	QT	52.377	16.254	3.359	3.161	1.074	0.308	1.521	5.425	12.057	0.195	4.632	100.363
YS-2	Yongshi farm	AOB	46.900	12.550	5.683	2.411	0.263	0.190	1.542	6.469	10.024	0.143	14.147	100.323
YS-3	Yongshi farm	AOB	46.869	12.326	6.553	2.434	0.464	0.137	1.417	6.450	11.516	0.162	11.926	100.254
YS-7	Yongshi farm	AOB	47.963	13.048	6.572	2.550	0.259	0.196	1.539	7.255	9.562	0.238	11.173	100.354
YF01	Yingfengling	BP	53.712	15.371	2.449	1.147	0.620	0.223	2.121	2.849	11.009	0.211	10.813	100.525
YF02	Yingfengling	BP	54.037	15.142	2.578	1.780	0.801	0.284	2.137	3.342	11.095	0.224	9.166	100.586
TY-1	Tianyang basin	OT	50.311	14.922	4.133	3.263	0.407	0.208	1.470	7.021	10.995	0.160	7.303	100.192
TY-2	Tianyang basin	OT	51.386	14.990	4.009	3.547	0.699	0.204	1.358	7.010	10.274	0.157	6.584	100.218
TY-3	Tianyang basin	OT	51.038	14.753	3.940	3.591	0.549	0.222	1.407	7.270	10.432	0.163	6.868	100.233
TY-4	Tianyang basin	OT	50.780	14.042	4.180	3.651	0.899	0.206	1.458	7.631	9.373	0.155	7.870	100.245
TY-10	Tianyang basin	OT	51.552	13.963	4.653	3.676	0.897	0.214	1.468	7.697	9.504	0.152	6.441	100.218

Rock type: AOB: alkali olivine basalt; OT: olivine tholeiite; QT: quartz tholeiite; BP: Basaltic pyroclastic.

field (>80 km), revealing an origin from the mantle (Han et al., 2009). The enrichment of light rare earth elements in basaltic pyroclastic rocks, alkaline olivine basalts, olivine tholeiites, and quartz tholeiites decreases in that order.
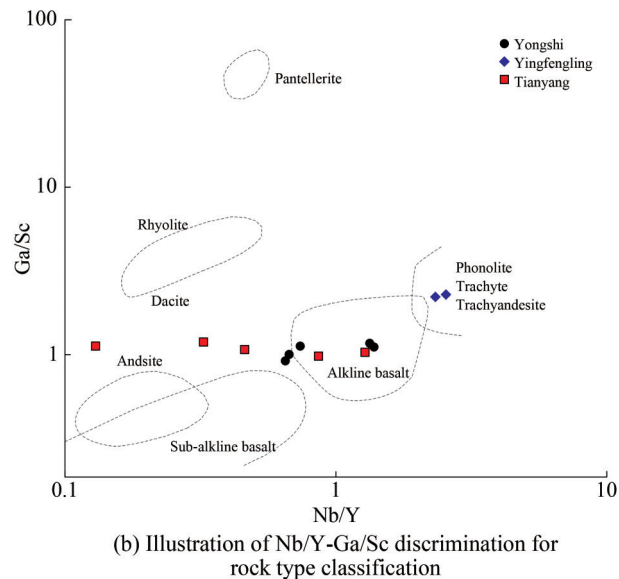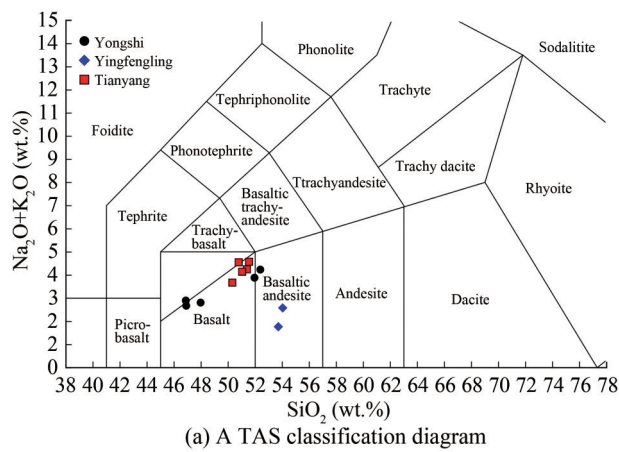
4.2 Water chemistry

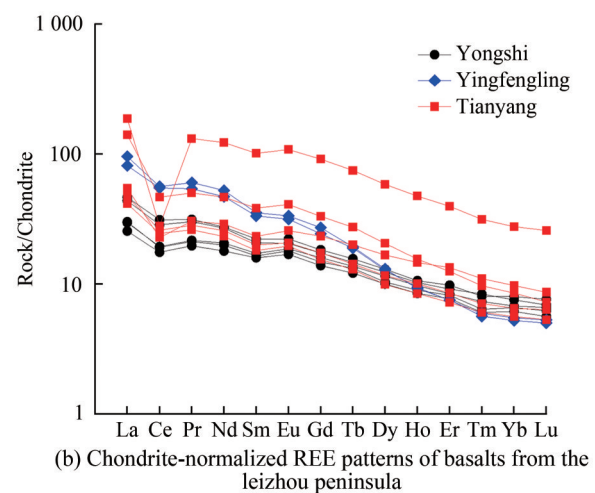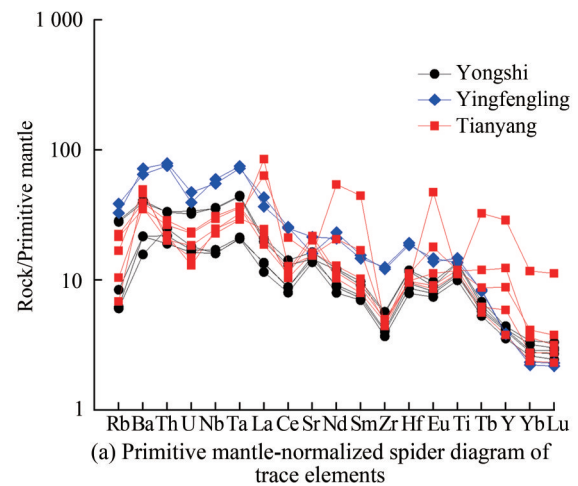Table 5 lists the analytical results of the aqueous ionic composition. The pH values of aqueous solutions vary from 7.0 to 8.0, with an average value of 7.6. The Yingfengling and Yongshi Farm sites predominantly comprise neutral groundwater, while the Tianyang Basin site is predominantly weakly alkaline. The numerous soluble ions in the weathered basalts runoff in the presence of abundant rainfall in the sampling area, yielding low-salinity water samples. The total hardness of the water samples ranges

Table 4 Results of trace and rare element compositions of basalt samples from the candidate sites in the Leizhou Peninsula

Sample	Sc	V	Cr	Ni	Cu	Zn	Rb	Sr	Y	Zr	Nb	Ba	La	Ce	Nd	Pb	Th	U
YS-1	20.4	168.60	366.9	245.7	89.04	130.0	17.71	305.0	18.21	62.55	25.18	273.40	13.52	23.06	16.14	5.38	2.84	0.71
YS-1-2	19.8	185.70	376.3	271.9	87.50	136.7	18.10	344.7	19.17	63.73	25.57	284.90	14.37	25.17	16.43	2.73	2.81	0.68
YS-2	21.4	178.00	650.5	236.8	68.88	107.6	3.94	302.0	18.04	46.00	12.13	151.20	9.18	15.66	12.39	2.08	1.86	0.36
YS-3	17.3	151.60	568.8	200.9	61.35	100.0	5.33	287.8	15.40	41.19	11.38	150.60	7.90	14.17	10.75	3.71	1.61	0.34
YS-7	23.5	167.10	708.3	240.6	70.84	123.1	3.83	322.7	17.54	44.84	11.42	109.50	9.32	15.47	11.93	3.44	2.11	0.38
YF01	12.0	62.11	823.6	217.5	56.80	139.4	20.75	337.5	16.85	135.7	39.27	502.50	29.60	45.26	31.41	7.15	6.70	0.99
YF02	12.3	75.98	600.1	157.2	57.93	147.3	24.41	450.8	16.62	140.2	42.37	451.50	25.19	44.27	28.17	7.98	6.41	0.83
TY-1	21.8	182.30	796.6	277.5	73.85	169.5	4.34	326.5	53.52	52.45	17.38	322.80	43.51	37.52	27.90	2.28	1.87	0.27
TY-2	21.5	183.10	812.8	280.9	77.84	134.1	10.62	341.3	38.18	53.00	17.59	346.40	16.89	18.36	17.35	1.56	1.72	0.39
TY-3	19.7	169.80	726.3	262.9	63.97	132.5	6.59	324.8	125.2	49.32	16.25	251.30	57.99	22.59	73.35	1.58	1.70	0.31
TY-4	21.0	161.00	854.5	317.9	75.32	113.0	13.58	425.6	16.43	52.82	21.05	244.00	12.83	19.80	13.91	6.81	2.24	0.48
TY-10	23.5	168.90	1723.0	329.5	108.01	104.1	14.24	457.2	25.57	55.77	22.07	273.70	14.64	20.94	15.41	1.97	2.44	0.49

(a) A TAS classification diagram

(b) Illustration of Nb/Y-Ga/Sc discrimination for rock type classification

Figure 4 The composition and rock type classification of basalts from the Leizhou Peninsula

(a) Primitive mantle-normalized spider diagram of trace elements

(b) Chondrite-normalized REE patterns of basalts from the leizhou peninsula

Figure 5 Chondrite-normalized REE patterns of basalts and Primitive mantle-normalized spider diagram

$Mg^{2+} > Na^+ > K^+ > Fe^{2+}$, demonstrating the prevalence of Ca^{2+} and Mg^{2+}, with Ca^{2+} concentrations ranging from 4.7 mg/L to 14.1 mg/L and Mg^{2+} concentrations ranging from 5.7 mg/L to 8.3 mg/L, while Na^+ and K^+ concentration values were

from 38 mg/L to 83 mg/L, which is very soft to soft water. The average milligram concentrations of cations are $Ca^{2+} >$

Table 5 Ionic compositions of water samples in the candidate sites of the Leizhou Peninsula

Sample	Total hardness	pH	Na$^+$	K$^+$	Ca^{2+}	Cl$^-$	F$^-$	Mg^{2+}	Fe^{2+}	SO$_4^{2-}$ SO$_4^{2-}$	CO$_3^{2-}$ HCO$_3^-$	HCO$_3^-$ HCO$_3^-$
YFL-1	83	7.992	8.58	18.72	11.93	30.46	0.269 7	8.31		9.70		57.75
YFL-2		8.049	7.55	3.333	12.55	14.83	0.272					
YFL-3		7.651	8.02	6.973	9.264	12.41	0.260 1					
YS01	68	7.600	9.51	1.370	14.1	9.11		8.06	0.41	5.96		71.8
YS02	50	7.700	7.88	1.530	8.88	9.11		6.70				
LSC-1	38	7.016	5.22	7.016	6.458	11.18	0.220 4	5.70		3.5		91.4
LSC-2		7.028	4.99	2.377	6.791	10.03	0.127					
LSC-3		7.086	4.64	2.114	5.12	11.30	0.170 3					
LSC-4		7.088	5.66	2.372	4.713	8.889	0.155					

Note: Units of water chemistry parameters are in mg/L, except for dimensionless pH. SO$_4^{2-}$, HCO$_3^-$ pore fissure water data sources for YFL-1–YFL-3 samples (Wu et al., 2022), SO$_4^{2-}$, HCO$_3^-$, and Cl$^-$ data sources for LSC-1–LSC-4 samples (Yao et al., 2007).

generally below 10 mg/L. The variation range of the cation contents of Ca^{2+}, Mg^{2+}, and Na$^+$ is small, whereas those of the anions such as Cl$^-$ (8.8–30.5 mg/L) are large. Cl$^-$ is the most stable ion in the groundwater because it is not adsorbed on the surface of the soil particles; thus, precipitating this ion is difficult. Therefore, the variation ranges of Cl$^-$ are possibly attributed to the seawater recharge of groundwater and artificial pollution.

Figure 6 displays the available types of aqueous solutions. Groundwater in the Leizhou Peninsula is primarily of the Mg−Ca−HCO$_3$ type, with less of the K−Na−Mg−HCO$_3$ type. Na$^+$/(Na$^+$+Ca^{2+}) and Cl$^-$/(Cl$^-$+HCO$_3^-$) are both less than 0.5, and the water-bearing medium in the Leizhou Peninsula is mainly basalts, which are rich in plagioclase, pyroxene, and other silicate minerals. This finding indicates that the weathering of basalts and the dissolution of Ca–Mg–Fe carbonate play a dominant role in affecting the hydrochemistry of groundwater on the Leizhou Peninsula. The water-bearing medium comprises basalts, which are rich in plagioclase, pyroxene, and other silicate minerals. Therefore, cations such as Ca^{2+} and Mg^{2+} are partially derived from the dissolution and release of weathered basalts. Additionally, other sources of cations include meteoric waters and deceased organisms.
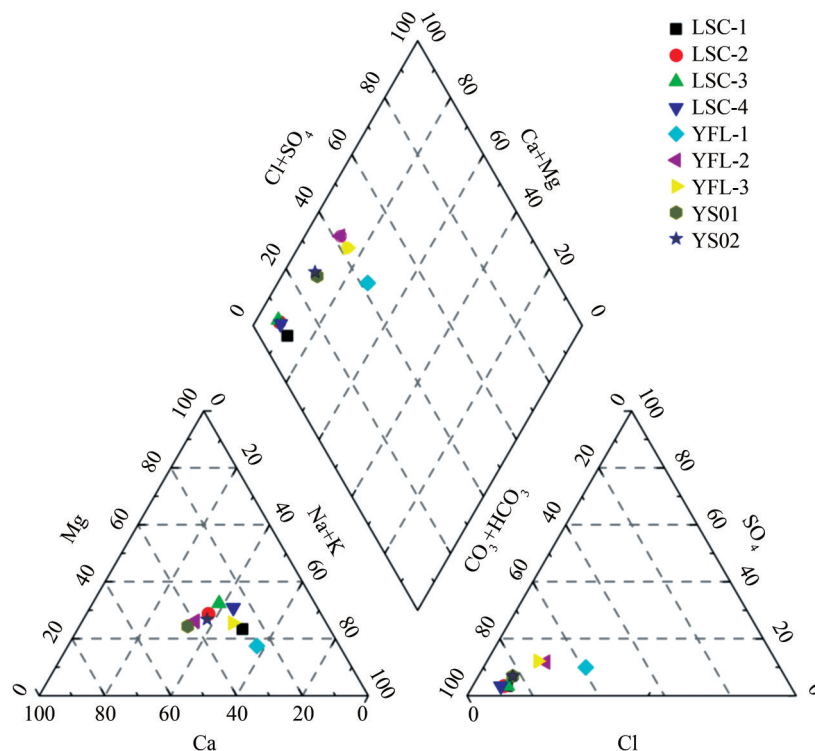
Figure 6 Water chemistry types of groundwater on the Leizhou Peninsula. Water samples collected from Yongshi Farm, Yingfengling, and Tianyang Basin on the Leizhou Peninsula are plotted in various patterns, and Piper's trilinear diagram is revised from Piper (1944)

4.3 Geochemical simulation

4.3.1 Model input parameters and CO₂ injection scheme

The precipitated minerals by the CO_2 mineralization reaction may be ankerite, calcite, magnesite, and siderite, depending on the relative abundance of the primary minerals in the basalts, the dissolution rate, and the thermodynamic stability of the carbonate minerals (Aradóttir et al., 2011; Gislason et al., 2014). Basalts from candidate areas (Yongshi Farm and Tianyang Basin) in the Leizhou Peninsula mainly comprise andesine, labradorite, anorthite, and pyroxene, with the sum volume fractions of the aforementioned minerals being more than 85% and also containing small amounts of fayalite and quartz. Different volume fractions of albite and anorthite were used to provide regular replacements for the entire plagioclase series and simplify the process of mineralization equilibrium calculation, eventually determining the components of primary minerals and their volume fractions involved in the geochemical simulation (Tables 6 and 7). The primary minerals included anorthite, albite, diopside, fayalite, and quartz, and the volume fractions were 54.6%, 36%, 6.6%, 1.3%, and 1.3%, respectively. Calcite, siderite, magnesite, dolomite, and dawsonite were considered secondary minerals based on the ions from the dissolution of primary minerals and the reaction equation. Table 5 shows the initial water composition used in the simulation, which included groundwater and natural springs from Yongshi Farm on the Leizhou Peninsula. Table 8 presents the basic coefficients used in this simulation. The input parameters, such as porosity, pH value, and permeability in the horizontal orientation, were directly obtained from the measured data of the samples. The simulation involved the injection of a mixture of pure CO_2 and H_2O in a ratio of 1:25 into CO_2 injection wells. These wells were located on the left side of the section, and the mixture flowed through the section. The total amount of injected CO_2 was 10 t, and the rate of mass injection was set at 3 m³/d for a period of five years in the simulation. The reaction path of CSBM was continuously observed for 20 years from the start of the injection.

4.3.2 Mineral variation results during CO₂ carbonation

The geochemical simulation results indicate that injecting a mixture of CO_2 and H_2O influences the chemical composition of rocks and aqueous solutions. This injection induced the dissolution of primary minerals such as albite, anorthite, diopside, and fayalite and the precipitation of quartz and secondary minerals such as calcite and magnesite (Figures 7(a) and (b), respectively). The injection of CO_2 will yield a weakly acidic aqueous solution, which will aid in the dissolution of primary minerals such as albite, anorthite, diopside, and fayalite. Positive ions (Ca^{2+}, Mg^{2+}, and Fe^{2+}) released will combine with dissolved CO_2 to form carbonate minerals, such as calcite, magnesite, siderite, and dolomite, as well as minor dawsonite. SiO_4^{2-} is released during this process to precipitate quartz. The dissolution rate of aluminum-bearing minerals, such as plagioclase, is slowest at neutral pH and increases at high pH conditions (Snæbjörnsdóttir et al., 2014, 2020). Therefore, albite and anorthite are less soluble at an initial pH of 7.6, resulting in lower concentrations of Al^{3+} and, consequently, less precipitation of dawsonite (Figure 7).

4.3.3 Reaction processes revealed by simulation outputs

Figure 8 shows changes in ion concentrations of subsurface fluid in 20 years after CO_2 injection. Metal cations, including Ca^{2+}, Mg^{2+}, and Fe^{2+}, display a similar trend, generally increasing during CO_2 injection and decreasing after injection cessation. The dissolution of diopside and fayalite contributes to the increase in Mg^{2+} and Fe^{2+} ion concentrations during CO_2 injection, and the precipitation rates of magnesite, siderite, and dolomite are stronger than the dissolution rate of diopside after CO_2 injection cessa-

Table 6 Dissolution reactions for minerals included in the reaction path calculations used in the simulation model.

CO₂ dissolution	$CO_2\ (g) = CO_2\ (aq)$ $CO_2\ (aq) + H_2O = HCO_3^- + H^+$ $HCO_3^- = H^+ + CO_3^{2-}$
Albite	$NaAlSi_3O_8 + 4H^+ = Na^+ + Al^{3+} + 2H_2O + 3SiO_2$
Anorthite	$CaAl_2Si_2O_8 + 8H^+ = Ca^{2+} + 2Al^{3+} + 4H_2O + 2SiO_2$
Labradorite	$(Ca,\ Na)\ Al\ (Al,\ Si)\ Si_2O_8 + 4H^+ = Na^+ + Ca^{2+} + 2Al^{3+} + 2H_2O + 3SiO_2$
Pyroxene	$(Mg,\ Fe)\ (SiO_3)_2 + 4H^+ = (Mg,\ Fe)^{2+} + 2H_2O + 2SiO_2$
Olivine	$(Mg,\ Fe)_2SiO_4 + 4H^+ = 2\ (Mg,\ Fe)^{2+} + 2H_2O + SiO_2$
Quartz	$SiO_2 + 2H_2O = H_4SiO_4$
Calcite	$CaCO_3 + H^+ = Ca^{2+} + HCO_3^-$
Siderite	$FeCO_3 + H^+ = Fe^{2+} + HCO_3^-$
Magnesite	$MgCO_3 + H^+ = Mg^{2+} + HCO_3^-$
Dolomite	$CaMg\ (CO_3)_2 + 2H^+ = Ca^{2+} + 2HCO_3^- + Mg^{2+}$
Dawsonite	$NaAlCO_3\ (OH)_2 + H^+ = Na^+ + Al\ (OH)_2^+ + HCO_3^-$

Table 7 Mineral composition in volume fractions in the simulation

	Mineral	Chemical formula	Volume percent (%)
Primary mineral	Anorthite	$NaAlSi_3O_8$	54.6
	Albite	$CaAl_2Si_2O_8$	36.0
	Diopside	$CaMg(SiO_3)_2$	6.6
	Fayalite	Fe_2SiO_4	1.3
	Quartz	SiO_2	1.3
Secondary mineral	Calcite	$CaCO_3$	0
	Siderite	$FeCO_3$	0
	Magnesite	$MgCO_3$	0
	Dolomite	$CaMg(CO_3)_2$	0
	Dawsonite	$NaAlCO_3(OH)_2$	0

Table 8 Parameters of basalts and aqueous phase used in the simulation model

Property	Value
Density of rock at 25 °C (g/cm³)	2.6
Density of water at 25 °C (kg/m³)	1.1
Permeability in horizontal orientation (mD)	8
Permeability in vertical orientation (mD)	40
pH	7.6
Pressure (kPa)	3 000
Porosity (%)	20
Temperature (°C)	40

tion, promoting a further reduction in Mg^{2+} and Fe^{2+} ion concentrations. The aluminum in the formation mainly existed as Al^{3+} at a pH below 5. However, as the reaction continued, the formation fluid gradually shifted from an acidic to a weakly acidic or moderately alkaline environment with a pH above 6. The aluminum in the formation mainly existed as $Al(OH)_4^-$ during this time, leading to a rapid decrease in Al^{3+}. With the dissolution of CO_2 into water, the concentration of HCO_3^- rapidly decreases, dissociating H^+ and CO_3^{2-}, causing a rapid reduction in the pH value near the injection well during CO_2 injection. Simultaneously, CO_3^{2-} reacts with metal cations, facilitating the rapid precipitation of carbonate minerals. The abundance of metal cations in primary minerals affects the precipitation of secondary minerals. The dissolution rates of aluminum-free minerals such as fayalite and diopside continue to decrease with increasing pH (Snæbjörnsdóttir et al., 2020), and the dissolution rates of fayalite and diopside continue to increase and decrease during the periods of CO_2 injection and CO_2 injection cessation, respectively. After CO_2 injection, the dissolution rate of anorthite gradually increased, and a small amount of quartz was generated (Figure 9(a)), and the dissolution rates of fayalite and diopside slowed down and gradually reached equilibrium (Figure 9(b)). Therefore, the pre-

(a) Changes in primary minerals

(b) Changes in secondary minerals
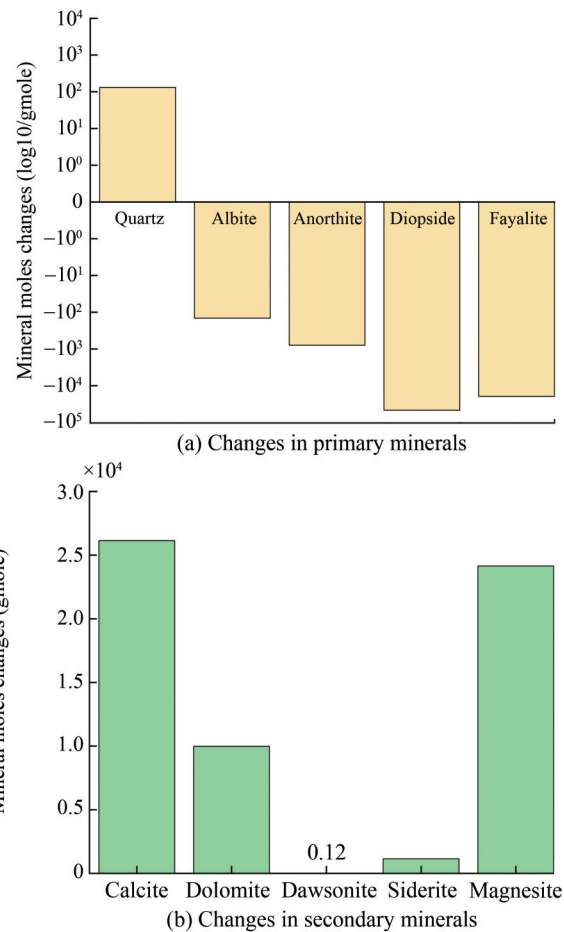
Figure 7 Mineral variations for 20 years calculated by the geochemical simulation in the basalts of the Leizhou Peninsula
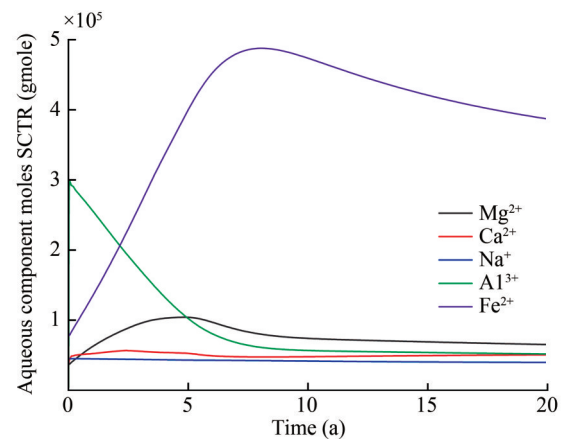
Figure 8 Simulated evolution of ion concentrations in basalts after CO_2 injection
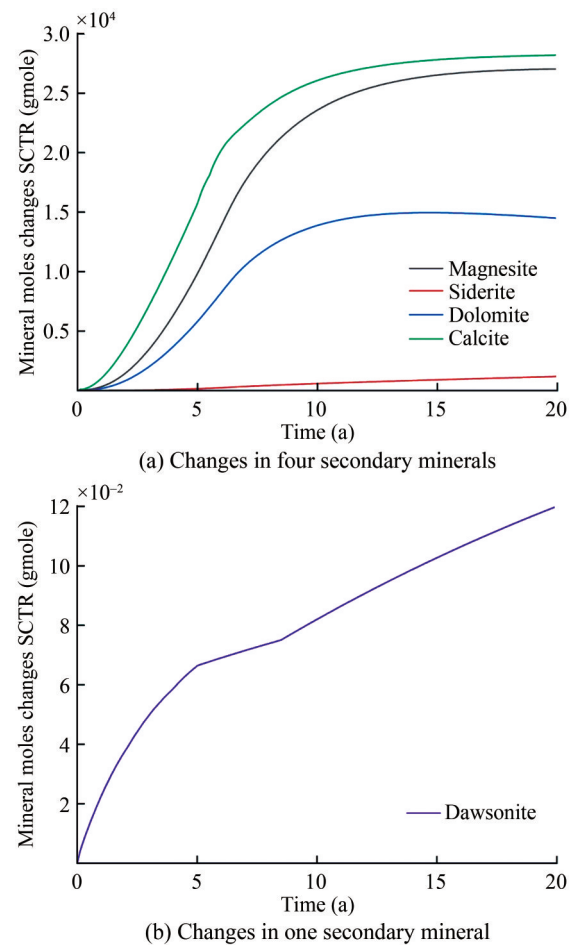
cipitation rates of calcite, dolomite, and magnesite also decreased once diopside reached dissolution equilibrium after cessation of CO_2 injection (Figure 10(a)), and a very small amount of dawsonite was precipitated (Figure 10(b)).

In addition to the effects on the minerals and the geological environment, CO_2 injection also caused changes in the

(a) Changes in three primary minerals

(b) Changes in two primary minerals
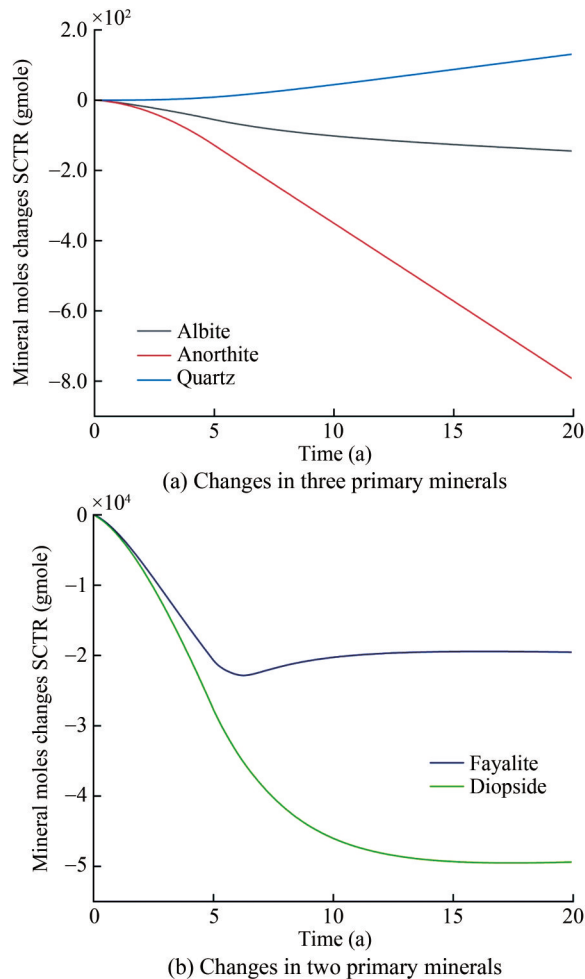
Figure 9 Simulated evolution of primary minerals molar quantities in basalts after CO_2 injection (positive values for minerals are precipitation; negative values are dissolution)

(a) Changes in four secondary minerals


(b) Changes in one secondary mineral

Figure 10 Simulated evolution of secondary minerals molar quantities in basalts after CO_2 injection (positive values for minerals are precipitation; negative values are dissolution)

pore mechanics and the solution environment of basalts. CO_2 injection induces an acidic environment, resulting in a rapid decline in fluid pH (Figure 11(a)). A pH minimum of 5.63 is observed during this stage, indicating the swift mineralization of most CO_2 near the injection well. Upon cessation of CO_2 injection, gradual reactions between CO_2 and HCO_3^- occur in proximity to the injection wells, resulting in an increase in alkaline pH that extends along the direction of production wells (Figures 11(b), (c), and (d)), which is consistent with pH results from geochemical modeling of CO_2 storage conducted by Alfredsson et al. (2013) at Hellisheidi Geothermal Power Plant, Iceland. This finding reveals the rapid mineralization of most of the CO_2 near the injection wells. Simulation results reveal that the region experiencing pH changes includes the injection well area as well as the upper and middle sections of the reservoir. This finding indicates lateral migration and upward transport tendencies for reactive ions such as HCO_3^-. The pH values of most grid areas were highly stable, possibly due to the buffering effect of the dissolution of carbon-

ate and bicarbonate minerals interacting with CO_2 (Seisenbayev et al., 2023). The precipitation of carbonate minerals induced changes in the porosity of the rock units (He et al., 2020), while the transport of CO_2 caused changes in the precipitation position of secondary minerals, which influenced the porosity of the basalts. The simulation results indicated a slight decrease in the porosity of basalts from 20% to 19.8%. Thus, the dissolution of primary minerals in the layer is less than the precipitation of secondary minerals, which are precipitated and filled inside the pores. Important chemical effects that lead to reservoir densification include the dissolution of primary silicate minerals such as aluminosilicate minerals and the generation of quarzitic cementation generators, as well as carbonate minerals in basalt reservoirs. By contrast, reduced porosity may affect fluid migration and the capability to sequester CO_2 mineralization in basalts.

4.3.4 Comparison with CarbFix in iceland

The CarbFix project in Iceland is currently the only project in the world that has commercially sequestered CO_2 in basaltic rocks by mineralization. The regional geology of
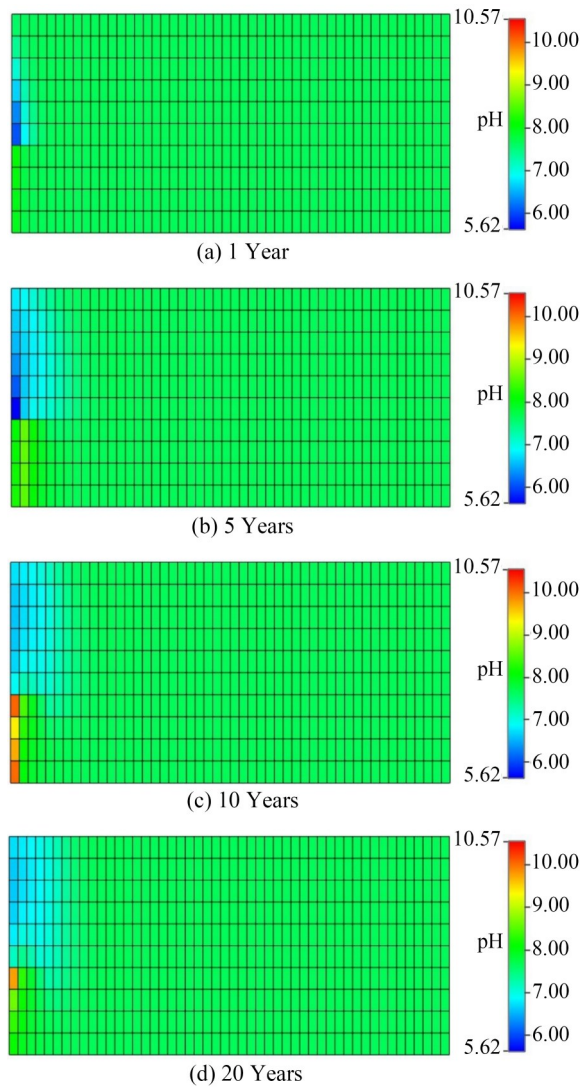
Figure 11 Changes of fluid pH value and distribution in basalt reservoir over time after CO_2 injection

the CarbFix project in Iceland has been monitored, and changes in the geological environment were modeled after CO_2 injection (Alfredsson et al., 2013). The simulation results of the CarbFix project show that consuming 1–1.8 mol of basalt vitrinite rapidly reduces the initial pH of 9.5 to a pH value of 3.5, which is similar to the pH variation induced by CO_2 injection around the injected well in the simulation. In the CarbFix project, at a pH value lower than 7–8, Ca–Mg–Fe carbonate and dolomite are the first secondary minerals to precipitate. Iron dolomite ($CaFe(CO_3)_2$) starts to precipitate at pH 8–9, and calcite finally starts to precipitate when the pH value finally rises to >9. Kaolinite and chalcedony continue to precipitate throughout the simulation and remain unaffected by changes in pH. Prediction results indicate that iron hydroxide ($Fe(OH)_3$) will start precipitating at pH values of 3.7 to 7 (Gysi and Stefánsson, 2011). However, the simulated secondary mineral precipitation in Leizhou Peninsula basalt is based on calcite as

the first batch of precipitated secondary minerals. Magnesite and dolomite then start to precipitate, while siderite precipitates in small amounts. Kaolinite and chalcedony precipitation are not observed during the entire process. The CarbFix project shows that more than 95% of the injected CO_2 is completely mineralized in less than two years, while the geochemistry simulation of the Yongshi Farm site on the Leizhou Peninsula shows that 36.8% of the injected CO_2 is fully mineralized within five years. This value has increased to 66.1% within 20 years (Figures 12(a) and (b)). Considerable differences generally exist between the CarbFix project and the Leizhou Peninsula basalts in terms of secondary mineral precipitation and the reaction process of CSBM. These differences in the simulation results of CO_2 storage by mineralization between the Leizhou Peninsula and the CarbFix project may be attributed to the following:
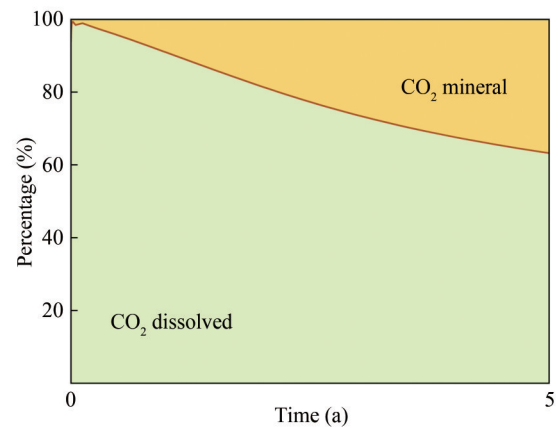
(a) Percentage of CO_2 reaction over simulation time at 5 years after the start of CO_2 injection
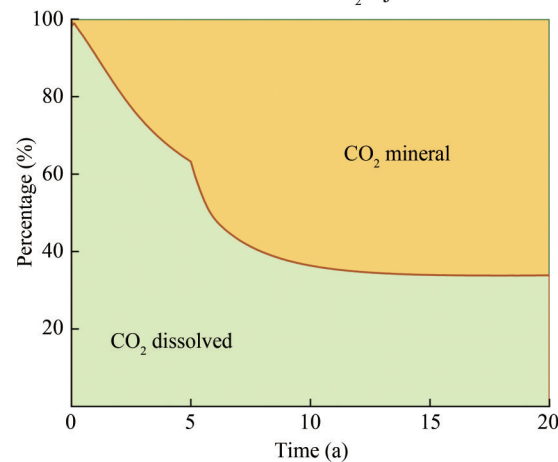
(b) Percentage of CO_2 reaction over simulation time at 20 years after the start of CO_2 injection

Figure 12 Percentage of CO_2 reaction over simulation time

1) Differences are found in the composition of primary minerals in the rock layers of the Leizhou Peninsula and the CarbFix project in Iceland. The basalts in the Leizhou

Peninsula comprise plagioclase (anorthite and albite), pyroxene (diopside), and a small amount of olivine and quartz, while the basalt formation of the CarbFix project is located at a depth of 400 m below ground. Basaltic glass accounts for more than 50% of the total, accompanied by minerals such as carbonate, montmorillonite, kaolinite, and quartz (Aradóttir et al., 2012). Therefore, in the CarbFix project simulation, the rate of dissolution precipitating Mg^{2+} and Fe^{2+} ion concentrations are fast, and Mg–Fe carbonate minerals are initially precipitated. However, the basalts of the Leizhou Peninsula contain high concentrations of albite, anorthite, and other plagioclase-series minerals that dissolve a high concentration of Ca^{2+}. The content of fayalite, which can precipitate Fe^{2+}, is extremely low and preferentially precipitates calcite.

2) The CarbFix project in Iceland assumed an initial pH of 9.5 at an alkaline condition, whereas the average pH of Yongshi Farm in the Leizhou Peninsula is 7.6, a neutral-weakly alkaline condition, and the dissolution rate peridotite > basalt vitrinite > diopside under acidic-neutral conditions; the difference in the dissolution rates of the three increases as the pH decreases (Snæbjörnsdóttir et al., 2020). Thus, the CarbFix project simulation rapidly precipitates Mg^{2+} and Fe^{2+} at first, whereas the minerals within the Leizhou Peninsula basalt slowly precipitate Mg^{2+} and Fe^{2+} in a neutral environment, eventually affecting the precipitated order and amount of secondary minerals. In addition, the porosity of basalt reservoirs in the CarbFix project in Iceland ranges from 5% to 40% (Franzson et al., 2008). Furthermore, the porosity of basalt reservoirs in the Leizhou Peninsula ranges from 11% to 28.9%, which is a considerable difference between the two areas. The porosity distribution affects the transport of ions and minerals in the basalts and further influences the reaction process and simulation results of CO_2 storage in basalts by mineralization.

4.4 Uncertainties associated with geochemical simulation

Uncertainties are generally associated with the geochemical simulations and are partly derived from the experimental data. In this study, input parameters such as pH value and porosity are taken as the laboratory-measured samples, which introduce minimal uncertainty. The crucial reaction parameters, including reactive surface area, activation energy, and the precipitation and dissolution rate of minerals, are also considered sources of uncertainties. The results of geochemistry simulations can demonstrate high uncertainties, occasionally reaching several orders of magnitude. These uncertainties can be reduced by selecting additional, specific sites and using precise physical and chemical parameters. The geological and hydrological conditions of Yongshi Farm and Tianyang sites are compared in this study, and the former is selected for the geochemistry simulation. Actual geologic sample parameters from the

sealed site are applied to represent the true conditions of the study area, approximate actual geological conditions, and minimize uncertainty. An improved understanding of the reaction mechanism and the factors that influence the reaction process is necessary to reduce uncertainties in reactive transport simulation. Further research is also required to perform a sensitivity analysis.

5 Conclusions

The basalt properties and hydrogeological conditions of the Leizhou Peninsula increase its suitability for CO_2 carbonation and successful storage in the rocks. The groundwater and natural spring water in the area are mainly neutral to weakly alkaline, with hydrochemistry dominated by the Mg–Ca–HCO_3 type. Water–rock interactions containing Mg–Ca minerals are believed to be the main reason for their formation. The basalts of the Leizhou Peninsula mainly comprise plagioclase, pyroxene, and Fe–Ti oxides, which account for over 85% of the total volume. These basalts also contain small amounts of olivine, quartz, and other minerals. These basalts are rich in divalent cations that can form carbonate minerals, with an average of approximately 6.2 moles of metal cations per 1 kg of rock. The geochemical simulation results indicate that the CSBM of the Leizhou Peninsula leads to the dissolution of minerals such as anorthite, albite, and diopside and the precipitation of secondary minerals such as calcite, dolomite, and siderite. The sequence of secondary mineral precipitation is calcite–Mg–Fe carbonate–Ca–Mg–Fe carbonate. The pH value initially decreased to 5.6 and then gradually increased to 10.6 around the injection well. The porosity slightly decreased, from 20% to 19.8%. The simulation results indicate that 66.1% of the injected CO_2 is completely mineralized within 20 years, demonstrating the potential of CSBM in the Leizhou Peninsula. The current study clarifies the influence of CSBM on regional geological characteristics and the CO_2 reaction model process. However, further investigation is necessary to determine the specific reaction mechanism of CSBM and implement the engineering project.

References

Alfredsson HA, Oelkers EH, Hardarsson BS, Franzson H, Gunnlaugsson E, Gislason SR (2013) The geology and water chemistry of the Hellisheidi, SW-Iceland carbon storage site. International Journal of Greenhouse Gas Control 12: 399-418. https://doi.org/10.1016/j.ijggc.2012.11.019

Aradóttir ESP, Sigurdardóttir H, Sigfússon B, Gunnlaugsson E (2011) CarbFix: a CCS pilot project imitating and accelerating natural CO_2 sequestration. Greenhouse Gases: Science and Technology 1(2): 105-118. https://doi.org/10.1002/ghg.18

Aradóttir ESP, Sonnenthal EL, Björnsson G, Jónsson H (2012) Multidimensional reactive transport modeling of CO_2 mineral sequestration in basalts at the Hellisheidi geothermal field. Iceland International Journal of Greenhouse Gas Control 9: 24-40. https://doi.org/10.1016/j.ijggc.2012.02.006

Bachu S (2015) Review of CO_2 storage efficiency in deep saline aquifers. International Journal of Greenhouse Gas Control 40: 188-202. https://doi.org/10.1016/j.ijggc.2015.01.007

Bachu S, Adams JJ (2003) Sequestration of CO_2 in geological media in response to climate change: capacity of deep saline aquifers to sequester CO_2 in solution. Energy Conversion and Management 44(20): 3151-3175. https://doi.org/10.1016/S0196-8904(03)00101-8

Bas MJL, Maitre RWL, Streckeisen A, Zanettin B (1986) A chemical classification of volcanic rocks based on the total alkali-silica diagram. Journal of Petrology 27(3): 745-750. https://doi.org/10.1093/petrology/27.3.745

Benson SM, Cole DR (2008) CO_2 sequestration in deep sedimentary formations. Elements 4(5): 325-331. https://doi.org/10.2113/gselements.4.5.325

Bryant E (1997) Climate process and change. Cambridge University Press, Cambridge, United Kingdom, 20-25. https://doi.org/10.1017/CBO9781139166751

Chen X, Chen L, Chen Y, Zeng G, Liu J (2014) Distribution summary of Cenozoic basalts in central and eastern China. Geological Journal of China Universities 20(4): 507. https://doi.org/10.16108/j.issn1006-7493.2014.04.002 (in Chinese)

Franzson H, Zierenberg R, Schiffman P (2008) Chemical transport in geothermal systems in Iceland: Evidence from hydrothermal alteration. Journal of Volcanology and Geothermal Research 173(3): 217-229. https://doi.org/10.1016/j.jvolgeores.2008.01.027

Galeczka I, Wolff-Boenisch D, Oelkers EH, Gislason SR (2014) An experimental study of basaltic glass–H_2O–CO_2 interaction at 22 and 50°C: Implications for subsurface storage of CO_2. Geochimica et Cosmochimica Acta 126: 123-145. https://doi.org/10.1016/j.gca.2013.10.044

Gislason SR, Broecker WS, Gunnlaugsson E, et al. (2014) Rapid solubility and mineral storage of CO_2 in basalt. Energy Procedia 63: 4561-4574. https://doi.org/10.1016/j.egypro.2014.11.489

Gislason SR, Wolff-Boenisch D, Stefansson A, Oelkers EH, Gunnlaugsson E, Sigurdardottir H, Sigfusson B, Broecker WS, Matter JM, Stute M, Axelsson G, Fridriksson T (2010) Mineral sequestration of carbon dioxide in basalt: A pre-injection overview of the CarbFix project. International Journal of Greenhouse Gas Control 4(3): 537-545. https://doi.org/10.1016/j.ijggc.2009.11.013

Goldberg DS, Takahashi T, Slagle AL (2008) Carbon dioxide sequestration in deep-sea basalt. Proceedings of the National Academy of Sciences 105(29): 9920-9925. https://doi.org/10.1073/pnas.0804397105

Gysi AP, Stefánsson A (2011) CO_2-water-basalt interaction. Numerical simulation of low temperature CO_2 sequestration into basalts. Geochimica et Cosmochimica Acta 75(17): 4728-4751. https://doi.org/10.1016/j.gca.2011.05.037

Han J, Xiong X, Zhu Z (2009) Geochemistry of Late-Cenozoic basalts from the Leiqiong area: The origin of the EM2 and contribution from sub-continental lithosphere mantle. Acta Petrological Sinica 25(12): 3208-3220. https://doi.org/10.1007/BF02943552 (in Chinese)

Hansen LD, Dipple GM, Gordon TM, Kellett DA (2005) Carbonated serpentinite (listwanite) at Atlin, British Columbia: A geological analogue to carbon dioxide sequestration. The Canadian Mineralogist 43(1): 225-239. https://doi.org/10.2113/gscanmin.43.1.225

He H, Tian C, Jin G, Han K (2020) Evaluating the CO_2 geological storage suitability of coal-bearing sedimentary basins in China. Environmental Monitoring and Assessment 192(7): 462. https://doi.org/10.1007/s10661-020-08424-w

Ho K, Chen J, Juang W (2000) Geochronology and geochemistry of late Cenozoic basalts from the Leiqiong area, southern China. Journal of Asian Earth Sciences 18(3): 307-324. https://doi.org/10.1016/S1367-9120(99)00059-0

Huang Z, Cai F (1994) A new approach to the Quaternary volcanicity in the Leiqiong area. Tropical geography 1: 1-10. https://doi.org/10.13284/j.cnki.rddl.000020 (in Chinese)

Huang Z, Cai F, Han Z, Chen J, Zong Y, Lin X (1993) The Quaternary Volcano of the Leiqiong area. Science Press, Beijing, China, 128-135. (in Chinese)

Jia B, Tsau J-S, Barati R (2019) A review of the current progress of CO_2 injection EOR and carbon storage in shale oil reservoirs. Fuel 236: 404-427. https://doi.org/10.1016/j.fuel.2018.08.103

Kong Z (2004) Hydrogeological property and laws of water abundance of the volcanic rocks in the Leizhou Peninsula. Tropical Geography 2: 136-139. https://doi.org/10.13284/j.cnki.rddl.000812 (in Chinese)

Li P, Jiang J, Cheng J, Zhao M (2023) Assessment of carbon dioxide mineralization sequestration potential of volcanic rocks in Leizhou Peninsula, Guangdong province, China. Geological Journal of China Universities 29(1): 76. https://doi.org/10.16108/j.issn1006-7493.2022078 (in Chinese)

Li W, Xu J, Jia L, Ma B, Chen J (2022) Research progress on key technologies of CO_2 storage in basalts. Hydrogeology & Engineering Geology 49(3): 164-173. https://doi.org/10.16030/j.cnki.issn.1000-3665.202107049 (in Chinese)

Li X, Chang C, Yu Q (2013) Model of basalt dissolution rate under CO_2 mineral sequestration conditions. Geoscience 27(6): 1477 (in Chinese)

Li X, Zhang Z, Li H, Zhang J, Bai X (2023) $^{40}Ar/^{39}Ar$ age of Quaternary volcanic rocks from the midwest of the Leizhou Peninsula, and their geologic significance. Journal of Geomechanics 29(4): 512-521. https://doi.org/10.12090/j.issn.1000-6616-2023098 (in Chinese)

Lu H, Lin C, Lin W, Liou T, Chen W, Chang P (2011) A natural analogue for CO_2 mineral sequestration in Miocene basalt in the Kuanhsi-Chutung area, Northwestern Taiwan. International Journal of Greenhouse Gas Control 5(5): 1329-1338. https://doi.org/10.1016/j.ijggc.2011.05.037

Lu Y, Tang C, Chen J, Chen J (2015) Groundwater Recharge and Hydrogeochemical Evolution in Leizhou Peninsula, China. Journal of Chemistry 2015: 1-12. https://doi.org/10.1155/2015/427579

Matter JM, Broecker WS, Stute M, Gislason SR, Oelkers EH, Stefánsson A, Wolff-Boenisch D, Gunnlaugsson E, Axelsson G, Björnsson G (2009) Permanent carbon dioxide storage into basalt: The CarbFix Pilot Project, Iceland. Energy Procedia 1(1): 3641-3646. https://doi.org/10.1016/j.egypro.2009.02.160

McDonough WF, Sun SS (1995) The composition of the Earth. Chemical Geology 120(3-4): 223-253. https://doi.org/10.1016/0009-2541(94)00140-4

McGrail BP, Schaef HT, Ho AM, Chien Y-J, Dooley JJ, Davidson CL (2006) Potential for carbon dioxide sequestration in flood basalts. Journal of Geophysical Research: Solid Earth 111(B12): B12201. https://doi.org/10.1029/2005JB004169

Oelkers EH, Cole DR (2008) Carbon dioxide sequestration: A solution to a global problem. Elements 4(5): 305-310. https://doi.org/10.2113/gselements.4.5.305

Oelkers EH, Gislason SR, Matter J (2008) Mineral carbonation of CO_2. Elements 4(5): 333-337. https://doi.org/10.2113/gselements.4.5.333

Pacala S, Al-Kaisi M, Barteau M, et al. (2018) Negative emissions technologies and reliable sequestration: a research agenda. National Academies of Sciences, Engineering, and Medicine, Washington, DC, USA. https://doi.org/10.17226/25259

Pham VTH, Lu P, Aagaard P, Zhu C, Hellevang H (2011) On the potential of CO_2–water–rock interactions for CO_2 storage using a modified kinetic model. International Journal of Greenhouse Gas Control 5(4): 1002-1015. https://doi.org/10.1016/j.ijggc.2010.12.002

Piper AM (1944) A graphic procedure in the geochemical interpretation of water-analyses. Eos, Transactions American Geophysical Union 25(6): 914-928. https://doi.org/10.1029/TR025i006p00914

Rutqvist J, Birkholzer J, Cappa F, Tsang C-F (2007) Estimating maximum sustainable injection pressure during geological sequestration of CO_2 using coupled fluid flow and geomechanical fault-slip analysis. Energy Conversion and Management 48(6): 1798-1807. https://doi.org/10.1016/j.enconman.2007.01.021

Sanna A, Uibu M, Caramanna G, Kuusik R, Maroto-Valer MM (2014) A review of mineral carbonation technologies to sequester CO_2. Chemical Society Reviews 43(23): 8049-8080. https://doi.org/10.1039/C4CS00035H

Seisenbayev N, Absalyamova M, Alibekova A, Leea W (2023) Reactive transport modeling and sensitivity analysis of CO_2–rock–brine interactions at Ebeity Reservoir, West Kazakhstan. Sustainability 15(19): 14434. https://doi.org/10.3390/su151914434

Snæbjörnsdóttir SÓ, Sigfússon B, Marieni C, Goldberg D, Gislason SR, Oelkers EH (2020) Carbon dioxide storage through mineral carbonation. Nature Reviews Earth & Environment 1(2): 2. https://doi.org/10.1038/s43017-019-0011-8

Snæbjörnsdóttir SÓ, Wiese F, Fridriksson T, Ármansson H, Einarsson GM, Gislason SR (2014) CO_2 storage potential of basaltic rocks in Iceland and the oceanic ridges. Energy Procedia 63: 4585-4600. https://doi.org/10.1016/j.egypro.2014.11.491

Sui S, Wang W (2003) Age exploration of the basal core from hole TY2 of the ancient Maar Lake in Tianyang, Guangdong province, China. Quaternary Science 23(2): 232 (in Chinese)

Tu K, Flower MFJ, Carlson RW, Zhang M, Xie G (1991) Sr, Nd, and Pb isotopic compositions of Hainan basalts (south China): Implications for a subcontinental lithosphere Dupal source. Geology 19(6): 567-569. https://doi.org/10.1130/0091-7613

White SK, Spane FA, Schaef HT, Miller QRS, White MD, Horner JA, McGrail BP (2020) Quantification of CO_2 Mineralization at the Wallula Basalt Pilot Project. Environmental Science & Technology 54(22): 14609-14616. https://doi.org/10.1021/acs.est.0c05142

Woodall CM, McQueen N, Pilorgé H, Wilcox J (2019) Utilization of mineral carbonation products: current state and potential. Greenhouse Gases: Science and Technology 9(6): 1096-1113. https://doi.org/10.1002/ghg.1940

Wu J, Wang Y, Hu Q, Ke X, Cheng J, Tang Z (2022) Hydrochemical characteristics and genetic analysis of groundwater in Leizhou Peninsula. Safety and Environmental Engineering 29(1): 145-153+162. https://doi.org/10.13578/j.cnki.issn.1671-1556.20210311 (in Chinese)

Yang M, Xie X, Chen J (2006) Sedimentary evidence and paleoenvironmental significance of the wetland of Tianyang Maar Lake, Leizhou Peninsula. Marine Geology Letters (7): 726-29+37. (in Chinese)

Yang S, Zheng Z, Zong Y, Li J, Huang K (2012) Characteristics and environmental significance of magnetic susceptibility of the Tianyang Maar Lake since Middle Pleistocene. Acta Scientia rum Naturalism Universitatis Sunya Seni 51(3): 121-127. (in Chinese)

Yao J, Zhou X, Li J, Dai W, Kang X (2007) Hydrogeochemical characteristics and evolution simulation of groundwater in basalts on the Leizhou Peninsula, Guangdong, China. Geological Bulletin of China 26(3): 327-334. (in Chinese)

Yu J, O'Reilly SY (2001) Iron-aluminium garnet megacrystals and parent magmatism in the Yingfengling Basalt, Leizhou Peninsula, China. Science Bulletin 46(6): 492-497. (in Chinese)

Zhang H, Wu Y, Luo W, Chen W, Liu H (2020) Hydrogeochemical investigations of groundwater in the Lingbei area, Leizhou Peninsula. Environmental Science 41(11): 4924-4935. https://doi.org/10.13227/j.hjkx.202002187

Zhang X, Ranjith PG (2019) Experimental investigation of effects of CO_2 injection on enhanced methane recovery in coal seam reservoirs. Journal of CO_2 Utilization 33: 394-404. https://doi.org/10.1016/j.jcou.2019.06.019